VIP ANR-09-COSI-03
Virtual Imaging Platform

D2.1.2: Object preparation workflows for the VIP

	(in alphabetical order)	
Hugues Benoit-Cattin	CREATIS	yougz@creatis.insa-lyon.fr
Sorina Camarasu-Pop	CREATIS	pop@creatis.insa-lyon.fr
Patrick Clarysse	CREATIS	clarysse@creatis.insa-lyon.fr
Germain Forestier	IRISA (INRIA Rennes)	germain.forestier@inria.fr
Denis Friboulet	CREATIS	friboulet@creatis.insa-lyon.fr
Bernard Gibaud	IRISA (INRIA Rennes)	Bernard.Gibaud@irisa.fr
Tristan Glatard	CREATIS	glatard@creatis.insa-lyon.fr
Patrick Hugonnard	CEA-Leti	patrick.hugonnard@cea.fr
Carole Lartizien	CREATIS	lartizien@creatis.insa-lyon.fr
Hervé Liebgott	CREATIS	liebgott@creatis.insa-lyon.fr
Adrien Marion	CREATIS	amarion@creatis.insa-lyon.fr
Joachim Tabary	CEA-Leti	joachim.tabary@cea.fr
Sébastien Valette	CREATIS	valette@creatis.insa-lyon.fr

Abstract

This deliverable describes object preparation workflows for integration in the Virtual Imaging Platform. These workflows convert object models from the VIP object format to the simulator native format, implementing scene definition, physical parameter adaptation and format conversions. They are described for the 4 simulators of the project, namely SIMRI (MRI), Sorteo (PET), Sindbad (CT) and FIELD-II (ultrasound).

Contents

1 Introduction

This deliverable is the second in VIP task T2.1., "Syntactic integration". It follows D2.1.1., "Prototype integration of simulators within VIP" [11]. The initial title proposed in the project description for this deliverable was "Benchmark of simulators w.r.t. parallelism exploitation". However a significant benchmarking activity was already performed in D2.1.1. since the porting of simulators to the grid infrastructure was faster than expected. The reader interested in detailed information and comments about this benchmark is invited to refer to the following pages of d2.1.1.:

- PET-Sorteo simulator: D2.1.1 Section 2.1, pages 7 and 8,
- Sindbad CT simulator: D2.1.1 Section 2.2.2, page 11 and 13,
- FIELD-II US simulator: D2.1.1 Section 2.3, page 15,
- SIMRI MRI simulatior: D2.1.1 Section 2.4, page 17 and 18.

Therefore the syntactic integration task of the project was extended to cover object preparation workflows in more details. This project deliverable describes our progresses and current solution for the syntactic integration of object models into multi-modality simulation workflows.

The term *object* is used here to describe anything that can potentially be the subject of an image simulation. For instance it covers biological models, geometrical phantoms

Name	Organ	Dimensions	Geometry parameters	Physical
Brainweb [1, 10]	brain	3D	voxels	MR only
Brainweb + MS lesions	brain	3D+t	voxels	MR only
Inflamed artery [4]	artery	3D+t	voxels	MR only
Adam [16]	thorax	3D+t	meshes and voxels	MR and PET
Zubal [27]	whole body	3D	voxels	PET,CT
Zubal + oncoPET tumors	whole body	3D	voxels	PET
XCAT [19]	whole body	3D	Nurbs	CT, PET

Table 1: Example of objects considered in VIP

and pure virtual models. Objects may include information related to time (movement and longitudinal follow-up), anatomy, pathology, contrast agents, external objects and physical parameters used by simulators. Table 1 shows object examples considered or being built in the project and Fig. 1 displays some of them.

An interface to publish and share objects among simulation users is currently being developed in the project (T2.3 - VIP client). Object preparation workflows aim at adapting these shared models to the simulators involved in a simulation scene. In particular these workflows consist of the following operations:

- Syntactical format conversions,
- Physical parameter generation for the considered image modalities,
- Geometrical transformation to the simulation scene.

Sections 2 to 4 describe the developed methods and choices for these 3 steps. Based on these, Section 5 presents object preparation workflows adapting objects to each of the native simulator formats.

2 Syntactical formats

2.1 VIP object format

Objects uploaded to the Virtual Imaging Platform are described in a particular format named IAMF for IntermediAte Model Format and developed by the project. Such a pivot format is meant to reduce the complexity of the conversion from external object formats to the formats used for simulator inputs. It also facilitates model sharing, browsing and vizualisation.

IAMF documents are `zip` files consisting of a set of data files augmented with an RDF document describing their content using annotations from the VIP ontology (see project milestone M1.2.2). Due to their wide adoption the VTK formats are preferred to describe the data files. An IAMF document can reference files of the following formats:

- VTK polydata (.vtp) files, for mesh description;
- VTK image (.mhd/.zraw) files, for object and physical parameter voxel maps;
- VTK unstructured grid (.vtu) files, for scatterer positions and amplitudes;

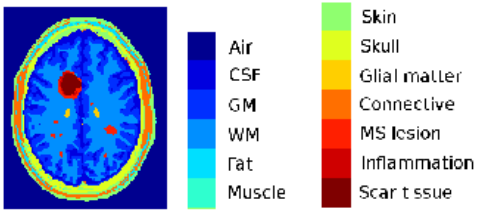

(a) Model of the inflamed brain (see task T3.3.)

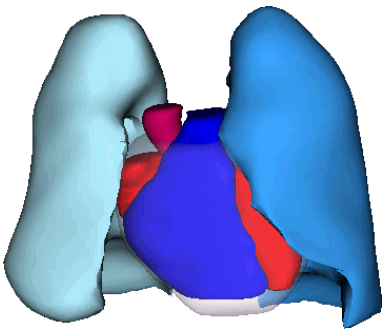

(b) ADAM thorax model

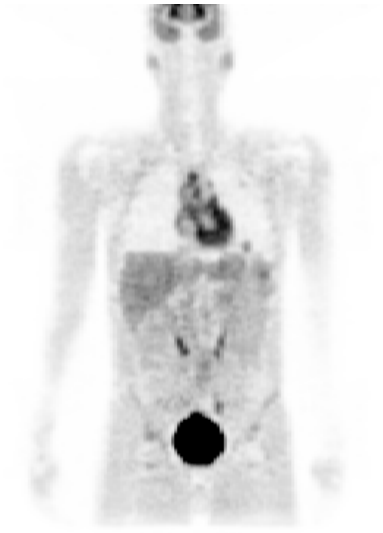

(c) Zubal whole-body model with tumors

Figure 1: Object examples

```
<Matters>
        <param tissu="Fat" Rho="73"  T1="754" T2="68"  Khi="0" />
        <Muscle Rho="70" T1="963" T2="60" Khi="0" />
        <Blood Rho="57" T1="1600" T2="100" Khi="0" />
        <Spin Rho="54" T1="350" T2="49"  Khi="0" />
        <SpinalCord Rho="56" T1="585" T2="70" Khi="0" />
        <Lung Rho="32" T1="1199" T2="56.5" Khi="0" />
        <Myocardium Rho="70" T1="1100" T2="50" Khi="0" />
        <Air Rho="0"  T1="0" T2="0"  Khi="0" />
</Matters>
```

Figure 2: Lookup table matching tissues to physical parameter values in SIMRI.

- Plain text and XML files for lookup tables.

RDF annotations organize these files in layers. A layer can be an object layer or a physical parameter layer. Object and physical parameter layers may be linked (but not necessarily). Object layers are distinguished as biological, pathological, contrast agent and external object layers.

Temporal information is associated to layers. Two time scales are distinguished. Time points reference a coarse time scale with a resolution in the order of a day. They are typically used to describe longitudinal follow-up studies. Instants reference a finer time scale with a resolution in the order of a second or less. They are used to describe movement, e.g., during the cardiac cycle.

This common format facilitates model sharing in the platform. Object preparation workflows can take a single object format as input and use fixed converters to map it to the native simulator input formats. The native simulator input formats are described in the next sub-section.

2.2 Simulator input formats

The interface of SIMRI was refactored to simplify the simulation of external objects. As a result the simulator as used in the project takes the following files as input:

- The object geometry is defined by a voxel map containing labels identifying tissues in VTK format;
- MR physical parameters are defined by look-up tables matching labels to tissue names and tissue names to physical parameter distributions. The latter is exemplified on Fig. 2;
- Simulator parameters, including object and physical parameter files are collected in a single text file.

Axes of the voxel map are aligned to the simulator frame and a translation vector can be used to shift the object w.r.t. the simulator.

In Sorteo the object geometry is defined in a voxel map of labels in the ECAT (.v file) format. Axes of the voxel map are aligned to the simulator frame. A translation vector can be used to shift the object w.r.t. the simulator and flips are also possible. A protocol text

file contains information about physical and geometrical parameters. For each emission label activity values are defined. Object labels are also matched to tabulated attenuation values.

In FIELD-II the object is defined by two arrays containing the list of scatterer positions (3D vectors) and amplitudes. These arrays are conveyed in a Matlab data file (`.mat`). Positions are expressed in the probe frame (the origin is the probe center).

In Sindbad the object is represented by meshes (.g file created from BRL-CAD software) and/or labeled voxels (.sdt/.spr files, equivalent to raw format). Correspondance between labels of voxels representation and tissue names is given by a tabulated file (.dat). For Monte Carlo computations, physical parameters are calculated from chemical composition with EGSnrc librairies and saved in a text file (.pegs4dat). Concerning analytical simulation, physical parameters are listed in another file (.tau) [2]. Geometric positioning of objects relative to the source and the detector is ensured by creating a .geo file permitting all possible affine movements.

3 Physical parameters

Physical parameters are required for each simulation modality, in particular:

- chemical compositions of tissues for PET and CT that will be used to calculate cross sections and probability of attenuation phenomena;
- magnetic properties (proton density, T1, T2, T2* and susceptibility) for MRI;
- echogenicity (spatial and amplitude distributions of scatterers) for ultrasound.

Determining these parameters is not always easy. Subsection 3.1 explains what are the main information sources and how they are integrated in the platform. Subsection 3.2 describes how the physical parameter values are used in the platform simulators.

3.1 Existing parameters sources

Depending on the modality information about physical parameters of biological tissues is available at various degrees. Chemical compositions can be found for more than 70 tissues in different articles. Schneider et al. [18] summarized values of density ρ and elemental weights in percentage points ω_i for major chemical elements such as hydrogen (H), carbon (C), nitrogen (N), oxygen (O), phosphorus (P) and calcium (Ca). Minor elements such as sodium (Na), magnesium (Mg), sulphur (S), chlorine (Cl), potassium (K) and iron (Fe) are not differentiated because their cumulated mass fraction is lower than 1%. The second source of information is the material database of PENELOPE [2] simulation software based on ESTAR program (NISTIR 4999, 1992). Finally, the third source is the database of the simulation software GATE [3]. Tissues for which we know chemical composition are listed in several tables in Appendix 1.1.

Magnetic properties are more difficult top obtain. Publications often focus on only one or two among the five parameters of interest (T1, T2, T2*, ρ and χ). Moreover these parameters depend on the magnetic field B_0. Consequently, we found data that are very heterogeneous. For example, two papers give parameters only for brain [26][6]. Another one provides values obtained from mouse, rat and bovine models [22] for several body parts. In these papers, the authors compare their values to numerous bibliographic

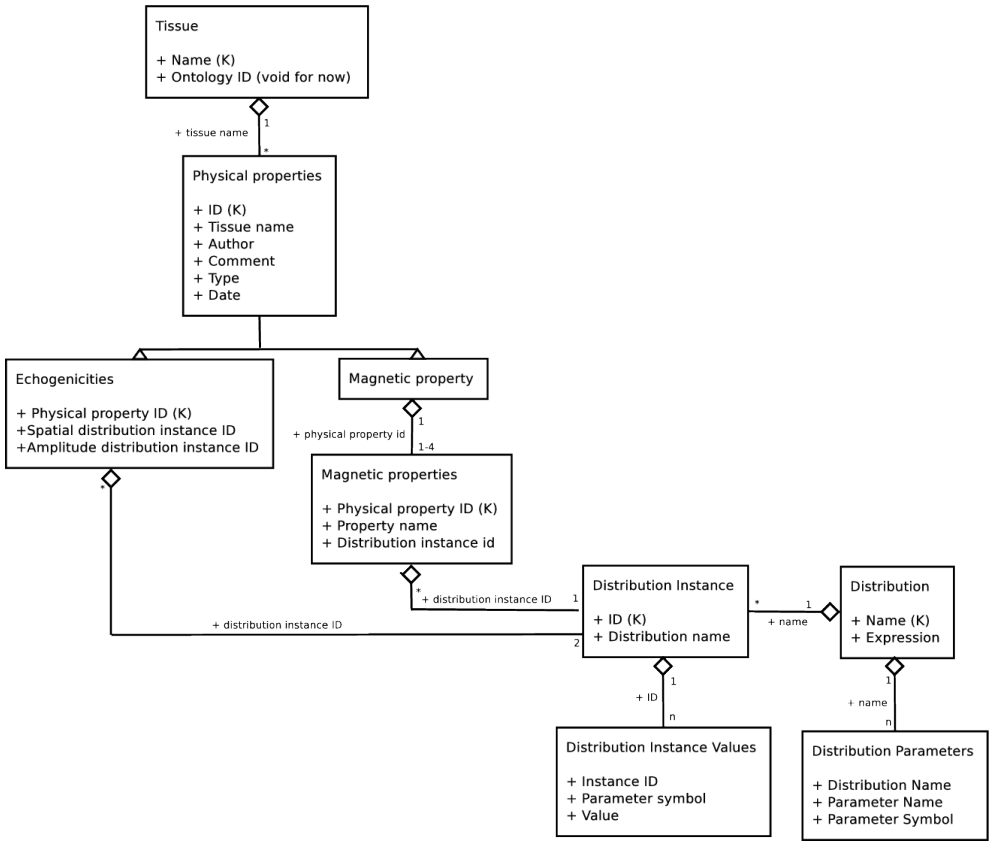

Figure 3: Schema of the physical parameter database.

references related to animal [15][5] and human models [13][9][14][20][21][12]. Finally, a model of inflamed artery based on [23] [17] using USPIO was proposed by Addy et al. [4]. Tissues for which we know magnetic parameters are listed in Appendix 1.2.

Knowing echogenicity parameters is also a complicated problem. Wagner et al. [25][24] showed that for fully developed speckle, *i.e.* assuming a minimum of 10 scatterers by resolution cell (FWHM), radio-frequwncy (RF) signal is Gaussian distributed and envelope signal is Rayleigh distributed. For partially developed speckle, Bernard et al. [7][8] showed that statistic of RF signal followed K distribution. They also use a generalized Gaussian to model partially or fully developed speckle with a unique formalism. Tissues for which we know echogenicity parameters are listed in Appendix 1.3.

A database was developed to store physical parameter values. When an object is uploaded to the platform it will be possible to use this database to retrieve physical parameters relevant for the simulation. This database could be populated either by manual upload or automatically by the object upload interface. The database schema is shown on Fig. 3. A tissue is identified by its name and its identifier in the VIP ontology (see project milestone M1.2.2). It may have one or several physical parameters. Physical parameters have a type that can be magnetic properties, chemical composition or echogenicity. Since different users may enter different parameter values, comment, author and edition date fields are also available. Property values are defined by statistical distributions. A distribution has a name and an expression and can have several parameters. A distribution instance then associates parameter values to these parameters.

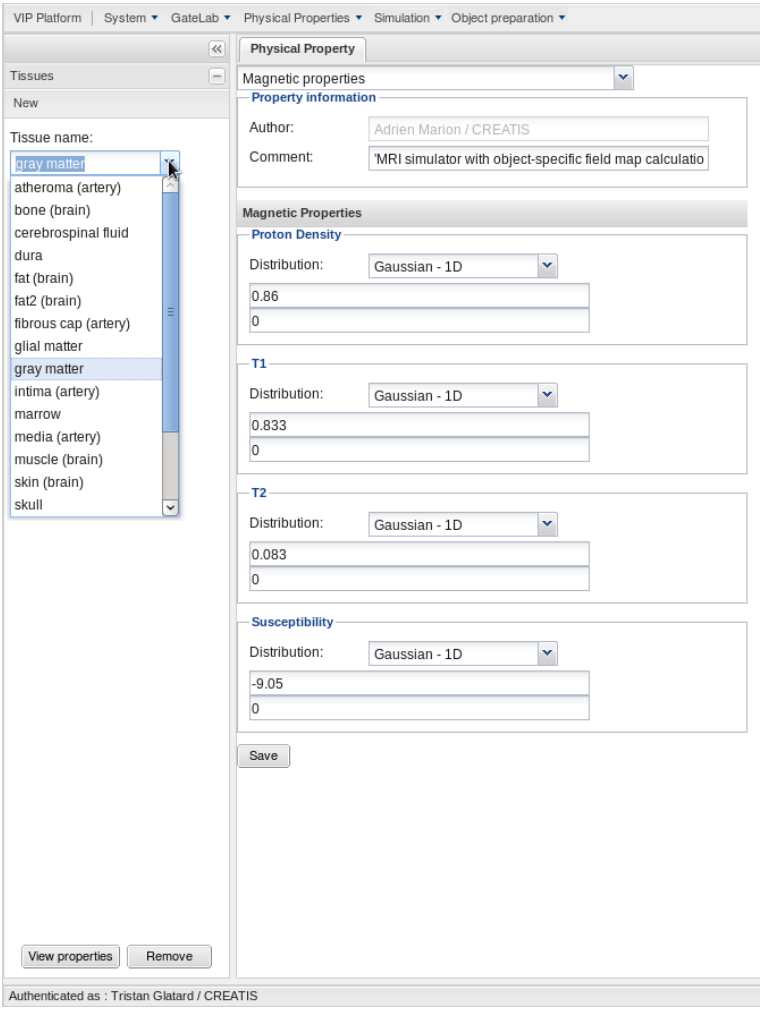

Figure 4: Interface of the physical parameter database.

A magnetic property is characterized by a set of magnetic properties that can be T1, T2, proton density, T2* or susceptibility. Each property is mapped to a distribution instance. Echogenicity values are defined by the spatial distribution of the scatterers and by their amplitude distribution. The chemical composition property is still under development. Fig. 4 shows a screenshot of this interface.

3.2 Generation of simulator inputs

The physical parameter values defined in the object model have to be adjusted to the native interface of the simulators. For SIMRI this operation is straightforward since the simulator directly takes magnetic property distributions as input.

FIELD uses scatterer lists. Thus, for each voxel, we generate a list of scatterers whose amplitudes and positions follow statistical laws defined in the database by its name and parameter values.

For Sindbad, it is a little bit more complicated because we need to generate two files (.tau used for analytical simulation and .pegs4dat used for Monte Carlo simulation). The .tau file is created with a sindbad routine from .tau files of chemical elements. These

files contain total cross sections, probability of photoelectric effect, Rayleigh scattering, Compton scattering and pair production. Concerning the .pegs4dat file, we have to create with a sindbad routine a .pegs4inp file that depends on cutoff energies (for photons and electrons) for each tissue. Then, we use pegs4 routine of EGSnrc to create the .pegs4dat file.

For Sorteo, we use the same process as for Sindbad and calculate, from the chemical composition given by the database, the total cross sections, probability of photoelectric effect, Compton scattering and Rayleigh scattering. Pair production effect is not considered by Sorteo. Currently, Sorteo uses a small database internal to the software and is not able to read these data files. We will have to modify the Sorteo code in a near future in order to read the text file containing parameters above.

4 Scene definition

A simulation scene must be defined before the simulation is launched. In addition to the object model this scene includes one or several imaging devices. These may be ultrasound probes, MR, CT or PET scanners.

4.1 Coordinate system

A device is defined by a source and a detector. Depending on the modality and simulator particularities may exist. In CT both are always distinguished while in US they are usually part of the same probe. In MR they may be distinguished in case B1 antenna profiles are considered by the simulator. For PET only the detector makes sense.

The scene is defined in a normalized coordinate system consisting of 3 frames (GKS standard). Fig. 5 displays this coordinate system. The object model is defined in an arbitrary `Rm` frame (`Om`,`i`,`j`,`k`). The position of the detector is defined by frame `Rd` (`Od`,`u`,`v`,`w`) where `Od`, `u`,`v` and `w` are given in `Rm`. The dimensions of a planar detector are given by (u_{max}, v_{max}) and (u_{min}, v_{min}) in `Rd`. Device coordinates in pixels (i.e. number and spacing between sensors) are specified if appropriate. The source is defined by frame `Rs` (`Os`,`p`,`q`,`r`) where `Os`, `p`,`q` and `r` are given in `Rm`.

The elements of `Rd` and `Rs` will be defined by the platform user *via* a dedicated graphical interface. This interface will specify geometrical conventions linking `Rs` and `Rd` to the physical characteristics of the simulators. This interface will be developed using the WebGL 3D API[1].

4.2 Instantiation on simulators

The graphical interface mentioned above will produce a rigid transformation (3 rotations and a 3D translation) for each imaging device. Rotations will be expressed using Euler angles. This information will be used differently for the simulators:

- For Sindbad the geometry parameter file will be directly edited;
- For SIMRI and Sorteo, the rotation parameters will be used to modify the voxel map and the translation parameters will be specified in the parameter files;

[1] http://www.khronos.org/webgl/

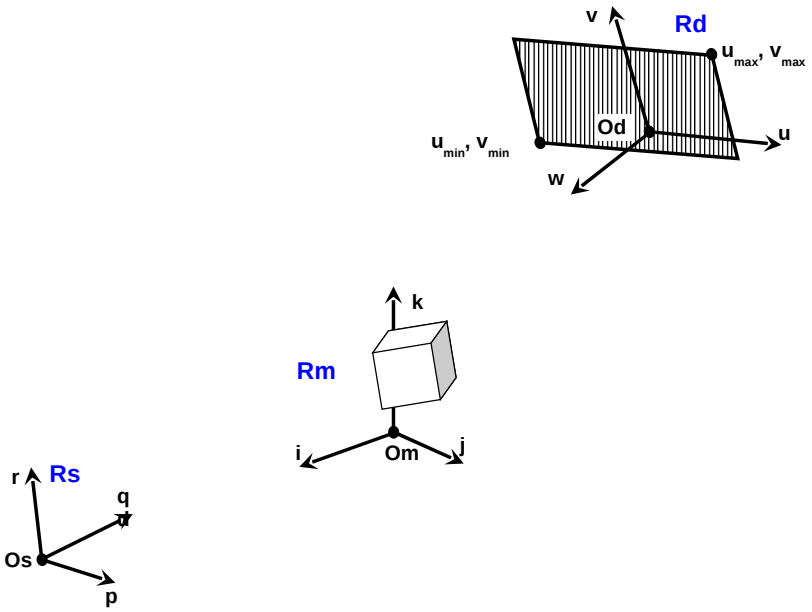

Figure 5: Normalized coordinate system used for scene definition.

- For FIELD-II a transformation matrix will be applied individually to the scatterers (see appendix B).

5 Object preparation workflows

Object preparation workflows for the 4 platform simulators are described on Fig. 6, 7, 8 and 9. These workflows implement syntactical format conversion, physical parameter generation and scene definition as described in the previous sections.

Each workflow takes as input an IAMF model that is assumed valid for the specific modality. This will be verified using the semantic model and associated rules.

Each of the 4 object preparation workflows consist on the same first steps, *i.e.* split time points and instants. Indeed, the IAMF model consists of [1..tp] time points and each time point consists of [1..i] instants. These two steps will create $tp * i$ `zip` files containing layers refered in the current instant with corresponding annotations. Each `zip` file refers to an instant of a time point will then be exploited separately.

For Sorteo, the workflow separates emission and attenuation processes. Concerning emission, a flattening step is performed to arrange the layers (see 2.1) described for the current instant. Flattening of layers related to attenuation is performed in parallel. From flattened emission data, we read nuclear activity and complete the protocol that will be used by Sorteo. Flattened emission data are also transformed using the geometrical transformation given by user. Finally, a format conversion step from zraw to ECAT format is realized to construct a .v file. From flattened attenuation data, we read labels associated to the labeled model to calculate cross sections and probabilities of attenuation phenomena

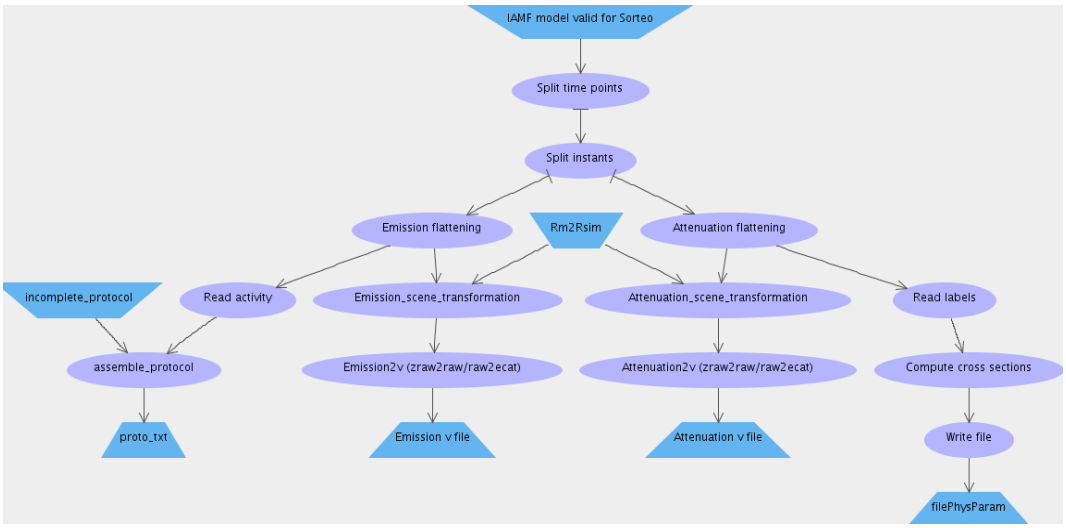

Figure 6: Object preparation workflow for PET simulator Sorteo.

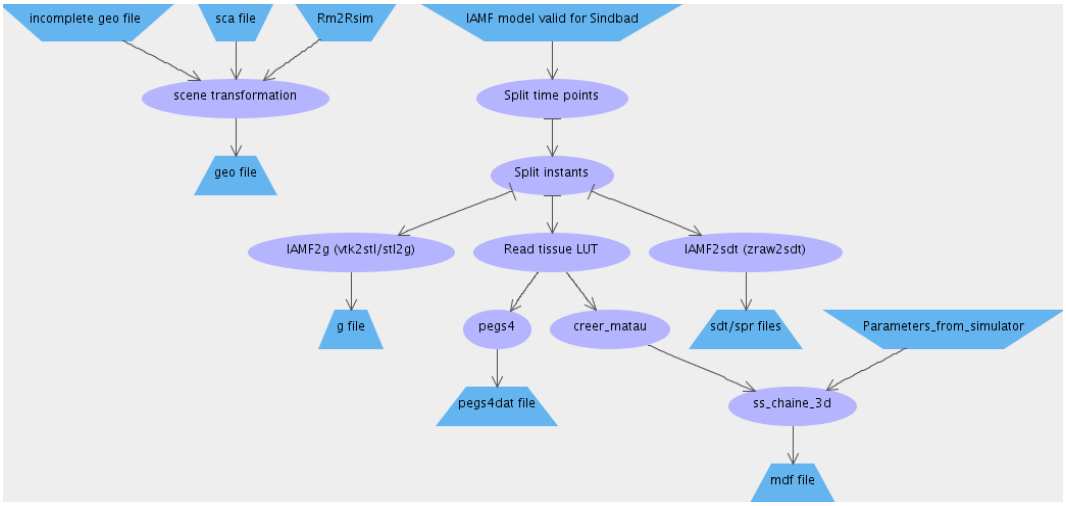

Figure 7: Object preparation workflow for CT simulator Sindbad.

(see 3.2) before writing them in a text file. Similarly to emission part, flattened attenuation data are geometrically transformed before to be converted in ECAT format.

For Sindbad, an independent step consists in updating the .geo file from the geometrical transformation provided by user and the scanner file (.sca). Separately, the `zip` file corresponding to an instant is used to convert mesh information to .g files with a BRL-CAD routine and voxel information to .sdt/.spr files with a sindbad routine. The last step reads the LUT linking labels to tissue names and uses pegs4 routine to construct the .pegs4dat file and `creer_matau` routine to construct .tau file containing cross sections and probabilities of attenuation phenomena. The .tau file is then combined with several simulator's paramters to write a .mdf file with a Sindbad routine `ss_chaine_3d`.

For Field II, the `zip` file is firstly flattened. Then, we use a query to test if a list of scatterers is embedded. If no, we read physical parameters, *i.e.* echogenicity distributions, from flattened object. We use them with sequence's parameters and the converted mat file (Matlab format) corresponding to voxelic labeled representation to generate scatterers.

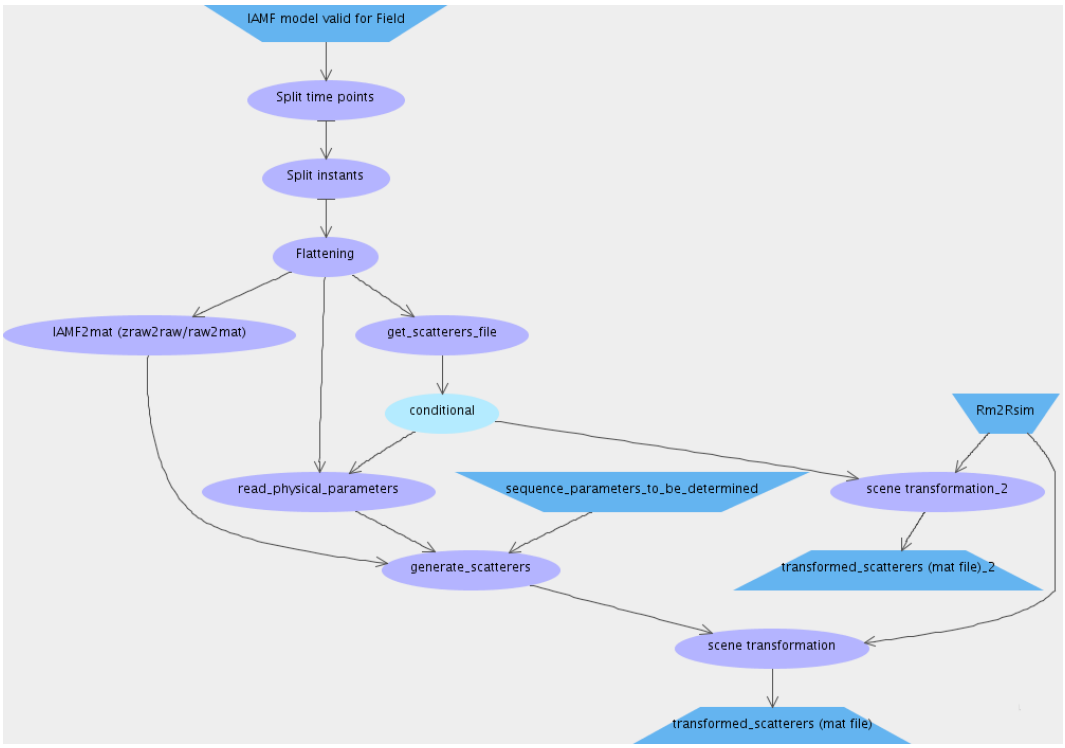

Figure 8: Object preparation workflow for ultrasound simulator FIELD-II.

Finally, this list of scatterers is transformed using geometrical transformation given by user. If a list of scatterers exist, it is only geometrically transformed.

For Simri, we extract LUT corresponding to tissues and generate the tissues to physical parameters file. After that, we flatten labeled volumes before to apply them the geometrical transformation. In parallel, physical parameters maps are extracted before to be flattened and transformed. Labeled volumes and physical parameters maps are then packed in a single `tgz` file that will be used by Simri.

6 Conclusion

Object preparation workflows were defined for the 4 simulators of the project. Their implementation is still on-going and will be available in the VIP platform in the coming months. These workflows are able to convert an object defined in the VIP object format into the native formats of the simulators.

Choices made to define the VIP object format (see section 2.1) are backed by a thorough dissemination effort in the simulation community. In particular presentations were made at the SIMED regional cluster initiative in November 2010 and a workshop was organized at the GDR STIC Santé in January 2011 to collect feedback about the information conveyed by the format. Therefore we hope that the platform could easily be extended to other simulation use-cases once in a mature state.

Material from this document will be submitted to the 2011 IEEE CBMS conference.

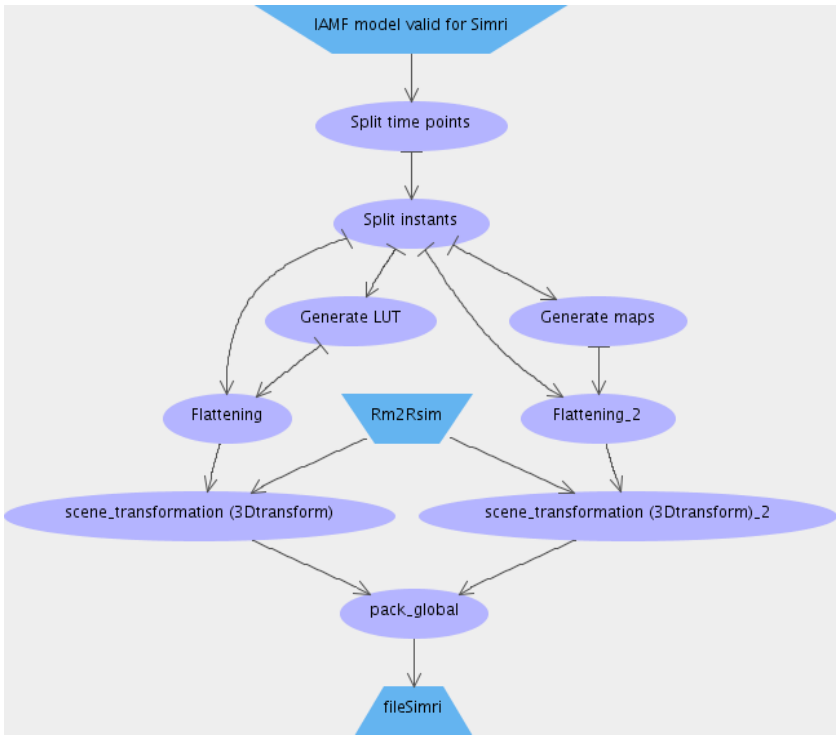

Figure 9: Object preparation workflow for MRI simulator SIMRI.

References

[1] http://mouldy.bic.mni.mcgill.ca/brainweb/.

[2] http://www.nea.fr/abs/html/nea-1525.html.

[3] http://opengatecollaboration.healthgrid.org/.

[4] O. Addy, D. Charpigny, M. Sigovan, E. Canet-Soulas, H. Benoit-Cattin, and D. Nishimura. MRI simulation framework for atherosclerosis inflammation with USPIOs. In *4th European Molecular Imaging Meeting*, Barcelona, Spain, May 2009.

[5] Thomas Aherne, Dimiter Tscholakoff, Walter Finkbeiner, Udo Sechtem, Nikita Derugin, Edward Yee, and Charles B. Higgins. Magnetic resonance imaging of cardiac transplants: the evaluation of rejection of cardiac allografts with and without immunosuppression. *Circulation*, 74:145–156, 1986.

[6] B. Aubert-Broche, A. C. Evans, and L. Collins. A new improved version of the realistic digital brain phantom. *Neuroimage*, 32:138–145, 2006.

[7] O. Bernard, J. D'Hooge, and D. Friboulet. Statistics of the radio-frequency signal based on K distribution with application to echocardiography. *IEEE Transactions on Ultrasonics, Ferroelectrics and Frequency Control*, 53(9):1689–1694, 2006.

[8] O. Bernard, B. Touil, J. D'Hooge, and D. Friboulet. Statistical modeling of the radiofrequency signal for partially and fully developed speckle based on a Generalized Gaussian model with application to echocardiography. *IEEE Transactions on Ultrasonics, Ferroelectrics and Frequency Control*, 54(10):2189–2194, 2007.

[9] A. Cieszanowski, W. Szeszkowski, M. Golebiowski D. K. Bielecki, M. Grodzicki, and B. Pruszynski. Discrimination of benign from malignant hepatic lesions based on their T2-relaxation times calculated from moderately T2-weighted turbo SE sequence. *European Radiology*, 12:2273–2279, 2002.

[10] D. L. Collins, A. P. Zijdenbos, V. Kollokian, J. G. Sled, N. J. Kabani, and C. J. Holmes A. C. Evans. Design and construction of a realistic digital brain phantom. *IEEE Transactions on Medical Imaging*, 17(3):463–468, June 2000.

[11] VIP ANR-09-COSI-03 consortium. D2.1.1: Prototype integration of simulators within VIP. Technical report, 2010.

[12] Thomas Ethofer, Irina Mader, Uwe Seeger, Gunther Helms, Michael Erb, Wolfgang Grodd, Albert Ludolph, and Uwe Klose. Comparison of longitudinal metabolite relaxation times in different regions of the human brain at 1.5 and 3 Tesla. *Magnetic Resonance in Medicine*, 50:1296–1301, 2003.

[13] N. Gelman, J. M. Gorell, P. B. Barker, R. M. Savage, E. M. Spickler, J. P. Windham, and R. A. Knight. MR Imaging of human brain at 3.0 T: preliminary report on transverse relaxation rates and relation to estimated iron content. *Neuroradiology*, 210:759–767, 1999.

[14] G. E. Gold, Eric Han, Jeff Stainsby, Graham Wright, Jean Brittain, and Christopher Beaulieu. Musculoskeletal MRI at 3.0 T: relaxation times and image contrast. *American Journal of Roentgenology*, 183:343–351, 2004.

[15] S. J. Graham, G. J. Stanisz, A. Kecojevic, M. J. Bronskill, and R. M. Henkelman. Analysis of changes in mr properties of tissues after heat treatment. *Magnetic Resonance Imaging*, 42:1061–1071, 1999.

[16] R. Haddad, P. Clarysse, M. Orkisz, D. Revel, and I. E. Magnin. A realistic anthropomorphic numerical model of the beating heart. *Innov Tech Biol Med - RBM*, 26(4):270–272, 2005.

[17] Joel Morrisett, Wesley Vick, Rakesh Sharma, Gerald Lawrie, Michael Reardon, Edward Ezell, Joseph Schwartz, Glen Hunter, and David Gorenstein. Discrimination of components in atherosclerotic plaques from human carotid endarterectomy specimens by magnetic resonance imaging ex vivo. *Magnetic Resonance Imaging*, 21:465–474, 2003.

[18] W. Schneider, T. Bortfeld, and W. Schlegel. Correlation between CT numbers and tissue parameters needed for Monte Carlo simulations of clinical dose distributions. *Physics in Medicine and Biology*, 45:459–478, 2000.

[19] W. P. Segars, B. M. Tsui, D. S. Lalush, E. C. Frey, M. A. King, and D. Manocha. Development and application of the new dynamic nurbs-based cardiac-torso (ncat) phantom. *Journal of Nuclear Medicine*, 42(5), 2001.

[20] John G. Sled and G. Bruce Pike. Quantitative imaging of magnetization transfer exchange and relaxation properties in vivo using MRI. *Magnetic Resonance in Medicine*, 46:923–931, 2001.

[21] Harvey E. Smith, Timothy J. Mosher, Bernard J. Dardzinski, Belinda G. Collins, Christopher M. Collins, Qing X. Yang, Vincent J. Schmithorst, and Michael B. Smith. Spatial variation in cartilage T2 of the knee. *Journal of Magnetic Resonance Imaging*, 14:50–55, 2001.

[22] G. J. Stanisz, E. E. Odrobina, J. Pun, M. Escaravage, S. J. Graham, M. J. Bronskill, and R. M. Henkelman. T1, T2 relaxation and magnetization transfer in tissue at 3T. *Magnetic Resonance Imaging*, 54:507–512, 2005.

[23] J-F Toussaint, G. M. LaMuraglia, J. F. Southern, V. Fuster, and H. L. Kantor. Coronary heart disease/atherosclerosis/myocardial infarction: Magnetic resonance images lipid, fibrous, calcified, hemorrhagic, and thrombotic components of human atherosclerosis in vivo. *Circulation*, 94(5):935–938, 1996.

[24] R. F. Wagner, M. F. Insana, and S. W. Smith. Fundamental correlation lengths of coherent speckle in medical ultrasonic images. *IEEE Transactions on Ultrasonics, Ferroelectrics and Frequency Control*, 35(1):34–44, 1988.

[25] R. F. Wagner, S. W. Smith, J. M. Sandrik, and H. Lopez. Statistics of speckle in ultrasound B-scans. *IEEE Transactions on Sonics and Ultrasonics*, 30(3):156–163, May 1983.

[26] D. A. Yoder, Y. Zhao, C. B. Paschal, and J. M. Fitzpatrick. MRI simulator with object-specific field map calculations. *Magnetic Resonance Imaging*, 22:315–328, 2004.

[27] I. G. Zubal, C. R. Harrell, E. O. Smith, and A. L. Smith. Two dedicated software, voxel-based, anthropomorphic (torso and head) phantoms. In P. J. Dimbylow (NRPB), editor, *Proceedings of the International Workshop*, pages 105–111, Chilton (UK), 1995.

A Physical parameters tables

1.1 Chemical compositions

Tissue name	Bibliographic sources
Adipose tissue	ESTAR (ICRP) / GATE (?)
Adipose tissue 1	Schneider, 2000
Adipose tissue 2	Schneider, 2000
Adipose tissue 3	Schneider, 2000
Adrenal gland	Schneider, 2000
Aorta	Schneider, 2000
Blood, whole	Schneider, 2000 / ESTAR (ICRP) / GATE (?)
Body	GATE (?)
Brain	ESTAR (ICRP) / GATE (?)
Brain, cerebrospinal	Schneider, 2000
Brain, grey matter	Schneider, 2000
Brain, white matter	Schneider, 2000
Breast	GATE (?)
C4 excl. cartilage (male)	Schneider, 2000
C4 incl. cartilage (male)	Schneider, 2000
Cartilage	Schneider, 2000 / GATE (?)
Clavicle, scapula	Schneider, 2000
Compact Bone	ESTAR (ICRU)
Connective tissue	Schneider, 2000
Cortical bone	Schneider, 2000 / ESTAR (ICRP)
Cranium	Schneider, 2000
D6, L3 excl. cartilage (male)	Schneider, 2000
D6, L3 incl. cartilage (male)	Schneider, 2000
Eye, lens	Schneider, 2000 / ESTAR (ICRP)
Femur (total bone)	Schneider, 2000
Femur (whole specimen)	Schneider, 2000
Femur, conical trochanter	Schneider, 2000
Femur, cylindrical shaft	Schneider, 2000
Femur, spherical head	Schneider, 2000
Gallbladder bile	Schneider, 2000

Tissue name	Bibliographic sources
Heart	GATE (?)
Heart 1	Schneider, 2000
Heart 2	Schneider, 2000
Heart 3	Schneider, 2000
Heart, blood filled	Schneider, 2000
Humerus (total bone)	Schneider, 2000
Humerus, cylindrical shaft	Schneider, 2000
Humerus, spherical head	Schneider, 2000
Humerus, whole specimen	Schneider, 2000
Innominate (female)	Schneider, 2000
Innominate (male)	Schneider, 2000
Intestine	GATE (?)
Kidney	GATE (?)
Kidney 1	Schneider, 2000
Kidney 2	Schneider, 2000
Kidney 3	Schneider, 2000
Liver	GATE (?)
Liver 1	Schneider, 2000
Liver 2	Schneider, 2000
Liver 3	Schneider, 2000
Lung	ESTAR (ICRP) / GATE (?)
Lung, blood-filled	Schneider, 2000
LungMoby	GATE (?)
Lymph	Schneider, 2000 / GATE (?)
Mammary gland 1	Schneider, 2000
Mammary gland 2	Schneider, 2000
Mammary gland 3	Schneider, 2000
Mandible	Schneider, 2000
Muscle	GATE (?)
Muscle, skeletal	ESTAR (ICRP)
Muscle, skeletal 1	Schneider, 2000
Muscle, skeletal 2	Schneider, 2000

Tissue name	Bibliographic sources
Muscle, skeletal 3	Schneider, 2000
Muscle, striated	ESTAR (ICRU)
Ovary	Schneider, 2000
Pancreas	Schneider, 2000 / GATE (?))
Prostate	Schneider, 2000
Red marrow	Schneider, 2000
RibBone	GATE (?)
Ribs 10th (male)	Schneider, 2000
Ribs 2nd, 6th (male)	Schneider, 2000
Sacrum (female)	Schneider, 2000
Sacrum (male)	Schneider, 2000
Skin	ESTAR (ICRP)
Skin 1	Schneider, 2000
Skin 2	Schneider, 2000
Skin 3	Schneider, 2000
Skull	GATE (?)
Small intestine (wall)	Schneider, 2000
SpineBone	GATE (?)
Spleen	Schneider, 2000 / GATE (?)
Sternum	Schneider, 2000
Stomach	Schneider, 2000
Testis	Schneider, 2000 / ESTAR (ICRP)
Thyroid	Schneider, 2000
Tissue, soft	ESTAR (ICRP)
Tissue, soft 4 components	ESTAR (ICRU)
Trachea	Schneider, 2000
Urine	Schneider, 2000
Whole vertebral column (male)	Schneider, 2000
Yellow marrow	Schneider, 2000
Yellow/red marrow (1 :1)	Schneider, 2000

1.2 Magnetic properties

Tissue name	Model	ρ	T1	T2	T2*	χ
Adventitia (artery)	human	?	[17] ?	[23]		?
Blood	human		[22][15]	[22][15]		
Blood (artery)	human	?	[17] ?	[17] ?		?
Bone	human	[26]	[26]	[26]		[26]
Cardiac Muscle	murine		[15]	[15]		
Cartilage	human		[14]	[14]		
Cartilage 0d	bovine		[22]	[22]		
Cartilage 55d	bovine		[22]	[22]		
Caudate head	human			[13]	[13] ?	
Cerebral hemisphere	murine		[15]	[15]		
Connective	human	[26]	[26]	[26]		[26]
Cortex (Prefrontal)	human			[13]	[13] ?	
CSF	human	[26][6]	[26][6]	[26][6]	[6]	[26]
Cystic lesions (liver)	human			[9]		
DURA	human	[6]	[6]	[6]	[6]	
External lipid (artery)	human	?	[17] ?	[17] ?		?
FAT (Brain)	human	[26][6]	[26][6]	[26][6]	[6]	[26]
FAT2 (Brain)	human	[6]	[6]	[6]	[6]	
Femur	human			[21]		
Fibrous cap (artery)	human	?	[17] ?	[23]		?
Focal nodular hyperplasia (liver)	human			[9]		
Glial Matter	human	[26]	[26]	[26]		[26]
Globus pallidus	human			[13]	[13] ?	
Gray Matter	human	[26][6]	[26][6][20]	[26][6][20]	[6]	[26]
Gray matter	bovine		[22]	[22]		
Gray Matter (Occipital)	human			[21]		

Tissue name	Model	ρ	T1	T2	T2*	χ
Heart	dog		[5]	[5]		
Heart	murine		[22]	[22]		
Hemagiomas (liver)	human			[9]		
Intima (artery)	human	?	[17] ?	[17] ?		?
Kidney	murine		[22]	[22]		
Lesions (brain)	human		[20]	[20]		
Lipid core (artery)	human	?	[17] ?	[23]		?
Liver	human			[9]		
Liver	murine		[22][15]	[22][15]		
Malignant lesions (liver)	human			[9]		
MARROW	human	[6]	[6]	[6]	[6]	
Marrow fat	human		[14]	[14]		
Media (artery)	human	?	[17] ?	[23]		?
Muscle	human		[14]	[14]		
Muscle (Brain)	human	[26][6]	[26][6]	[26][6]	[6]	[26]
Optic nerve	bovine		[22]	[22]		
Patella	human			[21]		
Plaque + USPIOhigh (artery)	human	?	?	?		[4]
Plaque + USPIOlow (artery)	human	?	?	?		[4]
Plaque + USPIOmed (artery)	human	?	?	?		[4]
Prostate	human		[15]	[15]		
Putamen	human			[13]	[13] ?	
Red nucleus	human			[13]	[13] ?	
Retroperitoneal adipose tissue	murine		[15]	[15]		
Skeletal muscle	murine		[22][15]	[22][15]		
Skin	human	[26]	[26]	[26]		[26]
SKIN/MUSCLE	human	[26][6]	[26][6]	[26][6]	[6]	[26]
SKULL	human	[6]	[6]	[6]	[6]	
Spinal cord	murine		[22]	[22]		
Subcutaneous fat	human		[14]	[14]		
Substantai nigra	human			[13]	[13] ?	
Synovid fluid	human		[14]	[14]		
Tibia	human			[21]		
VESSELS	human	[6]	[6]	[6]	[6]	
White Matter	human	[26][6]	[26][6][20]	[26][6][20]	[6]	[26]
White matter	bovine		[22][15]	[22][15]		
White matter (Frontal)	human			[13]	[13] ?	

1.3 Echogenicity properties

Tissue name	Parameters	Bibliographic sources
Myocardium	scatterers distribution	Bernard, 2007
Blood	scatterers distribution	Bernard, 2007

B Transformation matrix applied to the scatterers

We want to define rotation matrix corresponding to the geometrical transformation applied by user. For that, we access Euler angles with zxz convention. Euler rotations can be performed around moving axes or static axes if we invert rotations Thus, a xyz rotation with static axes ($R_{\theta_1,x}$, $R_{\theta_2,y}$, $R_{\theta_3,z}$) is equivalent to a $zy^{'}x^{''}$ rotation with moving axes ($R_{\theta_3,z}$, $R_{\theta_2,y'}$, $R_{\theta_1,x''}$).

In our particular case, we use a zxz convention with moving axes ($R_{\theta_{Z1},z}$, $R_{\theta_X,x'}$, $R_{\theta_{Z2},z''}$), which is equivalent to apply three successive rotations ($R_{\theta_{Z2},z}$, $R_{\theta_X,x}$, $R_{\theta_{Z1},z}$).

Let us now define the three canonic rotations as three matrices:

$$R_{\theta_{Z2},z} = \begin{pmatrix} cos\ \theta_{Z2} & -sin\ \theta_{Z2} & 0 \\ sin\ \theta_{Z2} & cos\ \theta_{Z2} & 0 \\ 0 & 0 & 1 \end{pmatrix}$$

$$R_{\theta_X,x} = \begin{pmatrix} 1 & 0 & 0 \\ 0 & cos\ \theta_X & -sin\ \theta_X \\ 0 & sin\ \theta_X & cos\ \theta_X \end{pmatrix}$$

$$R_{\theta_{Z1},z} = \begin{pmatrix} cos\ \theta_{Z1} & -sin\ \theta_{Z1} & 0 \\ sin\ \theta_{Z1} & cos\ \theta_{Z1} & 0 \\ 0 & 0 & 1 \end{pmatrix}$$

The global matrix defining the 3 successive rotations is then expressed by the product between the 3 matrices written above:

$$R = R_{\theta_{Z1},z} * R_{\theta_X,x} * R_{\theta_{Z2},z}$$

$$R = \begin{pmatrix} cos\ \theta_{Z1}\ cos\ \theta_{Z2} - sin\ \theta_{Z1}\ cos\ \theta_X\ sin\ \theta_{Z2} & -cos\ \theta_{Z1}\ sin\ \theta_{Z2} - sin\ \theta_{Z1}\ cos\ \theta_X\ cos\ \theta_{Z2} & sin\ \theta_{Z1}\ sin\ \theta_X \\ sin\ \theta_{Z1}\ cos\ \theta_{Z2} + cos\ \theta_{Z1}\ cos\ \theta_X\ sin\ \theta_{Z2} & -sin\ \theta_{Z1}\ sin\ \theta_{Z2} + cos\ \theta_{Z1}\ cos\ \theta_X\ cos\ \theta_{Z2} & -cos\ \theta_{Z1}\ sin\ \theta_X \\ sin\ \theta_X\ sin\ \theta_{Z2} & sin\ \theta_X\ cos\ \theta_{Z2} & cos\ \theta_X \end{pmatrix}$$

If we consider an additional translation defined by vector $T = [\Delta_x, \Delta_y, \Delta_z]^T$, the final transformation matrix is then given by:

$$M = \begin{pmatrix} cos\ \theta_{Z1}\ cos\ \theta_{Z2} - sin\ \theta_{Z1}\ cos\ \theta_X\ sin\ \theta_{Z2} & -cos\ \theta_{Z1}\ sin\ \theta_{Z2} - sin\ \theta_{Z1}\ cos\ \theta_X\ cos\ \theta_{Z2} & sin\ \theta_{Z1}\ sin\ \theta_X & \Delta_x \\ sin\ \theta_{Z1}\ cos\ \theta_{Z2} + cos\ \theta_{Z1}\ cos\ \theta_X\ sin\ \theta_{Z2} & -sin\ \theta_{Z1}\ sin\ \theta_{Z2} + cos\ \theta_{Z1}\ cos\ \theta_X\ cos\ \theta_{Z2} & -cos\ \theta_{Z1}\ sin\ \theta_X & \Delta_y \\ sin\ \theta_X\ sin\ \theta_{Z2} & sin\ \theta_X\ cos\ \theta_{Z2} & cos\ \theta_X & \Delta_z \\ 0 & 0 & 0 & 1 \end{pmatrix}$$